Linköping Studies in Science and Technology
Licentiate Thesis No. 1210

Spin splitting in open quantum dots and related systems

Martin Evaldsson

Linköpings universitet
INSTITUTE OF TECHNOLOGY

LIU-TEK-LIC 2005:65

Department of Science and Technology
Linköping University, SE-601 74 Norrköping, Sweden

Norrköping, 2005

Spin splitting in open quantum dots and related systems

Department of Science and Technology
Campus Norrköping, Linköping University
SE-601 74 Norrköping, Sweden

ISBN 91-85457-69-8 ISSN 0280-7971
Printed in Sweden by UniTryck, Linköping, 2005

Abstract

This thesis addresses electron spin phenomena in semi-conductor quantum dots/anti-dots from a computational perspective. In the first paper (paper I) we have studied spin-dependent transport through open quantum dots, i.e., dots strongly coupled to their leads, within the Hubbard model. Results in this model were found consistent with experimental data and suggest that spin-degeneracy is lifted inside the dot – even at zero magnetic field.

Similar systems were also studied with electron-electron effects incorporated via Density Functional Theory (DFT) in paper III. Within DFT we found a significant spin-polarisation in the dot at low electron densities. As the electron density increases the spin polarisation in the dot gradually diminishes. These findings are consistent with available experimental observations. Notably, the polarisation is qualitatively different from the one found in the Hubbard model – this indicates that the simplified approach to electron-electron interaction in the Hubbard model might not always be reliable.

In paper II we propose a spin-filter device based on resonant backscattering of edge states against a quantum anti-dot embedded in a quantum wire. A magnetic field is applied and the spin up/spin down states are separated through Zeeman splitting. Their respective resonant states may be tuned so that the device can be used to filter either spin in a controlled way.

Preface

This thesis summarises my first three years as a Ph.D. student at the Department of Science and Technology (ITN). It consists of two parts, the first serving as a short introduction both to mesoscopic transport in general and to the papers included in the second part. There are several persons to whom I would like to express my gratitude for help and support during these years:

First of all my supervisor Igor Zozoulenko for patiently introducing me to the field of mesoscopic physics and research in general, I have learnt a lot from you.

The other members in the Mesoscopic Physics and Photonics group, Aliaksandr Rachachou and Siarhei Ihnatsenka – it is great to have people around who actually understand what I'm doing.

Torbjörn Blomquist for providing an excellent C++ matrix library which has significantly facilitated my work.

A lot of people at ITN for various reasons, including Mika Gustafsson (everything), Michael Hörnquist and Olof Svensson (lunch company and company), Margarita Gonzáles (company and lussebak), Frédéric Cortat (company and for motivating me to run 5km/year), Steffen Ühlig (company and lussebak), Sixten Nilsson (help with teaching), Sophie Lindesvik (help with administrative issues).

Also a general thanks to all the past and present members of the 'Fantastic Five', and everyone who has made my coffee breaks more interesting.

I would also like to thank my parents and sister for being there, and of course my wife, Chamilly, for all her support, love and for proofreeding my English.

Finally, financial support from The Swedish Research Council (VR) and the National Graduate School for Scientific Computations (NGSSC) is acknowledged.

List of publications

Paper I: M. Evaldsson, I. V. Zozoulenko, M. Ciorga, P. Zawadzki and A. S. Sachrajda. Spin splitting in open quantum dots. *Europhysics Letters* **68**, 261 (2004)

Paper II: I. V. Zozoulenko and M. Evaldsson. Quantum antidot as a controllable spin injector and spin filter. *Applied Physics Letters* **85**, 3136 (2004)

Paper III: M. Evaldsson and I. V. Zozoulenko. Spin polarization in open quantum dots. Submitted for publication.

Contents

Chapter 1

Introduction

During the second half of the 20th century, the introduction of semiconductor materials came to revolutionise modern electronics. The invention of the transistor, followed by the integrated circuit (IC) allowed an increasing number of components to be put onto a single silicon chip. The efficiency of these ICs has since then increased several times, partly by straightforward miniaturisation of components. This process was summarised by Gordon E. Moore in the now famous "Moore's law", which states that the number of transistors on a chip doubles every second year[1]. However, as the size of devices continue to shrink, technology will eventually reach a point when quantum mechanical effects become a disturbing factor in conventional device design.

From a scientific point of view this miniaturisation is not troubling but, rather, increasingly interesting. Researchers can manufacture semiconductor systems, e.g., quantum dots or wires, which are small enough to exhibit pronounced quantum mechanical behaviour and/or mimic some of the physics seen in atoms. In contrast to working with real atoms or molecules, experimenters can now exercise precise control over external parameters, such as confining potential, the number of electrons, etc.. In parallel to this novel research field, a new applied technology is emerging – "*spintronics*" (spin electronics). The basic idea of spintronics is to utilise the electron spin as an additional degree of freedom in order to improve existing devices or innovate entirely new ones. Existing spintronic devices are built using ferromagnetic components – the most successful example to date is probably the read head in modern hard disk drives (see e.g., [22]) based on the Giant Magneto Resistance effect[2, 10].

Because of the vast knowledge accumulated in semiconductor technology there is an interest to integrate future spintronic devices into current semiconductor ones. This necessitates a multitude of questions to be answered, e.g.:

[1] Moore's original prediction made in 1965 essentially states (here slightly reformulated), that "*the number of components on chips with the smallest manufacturing costs per component doubles roughly every 12 months*"[18]. It has since then been revised and taken on several different meanings.

can spin-polarised currents be generated and maintained in semiconductor materials, does spin-polarisation appear spontaneously in some semiconductor systems?

Experiments, however, is not the only way to approach these new and interesting phenomena. The continuous improvement of computational power together with the development of electron many-body theories such as the Density Functional Theory provide a basis for investigating these questions from a theoretical/computational point of view. Theoretical work may explain phenomena not obvious from experimental results and guide further experimental work. Modelling of electron transport through semiconductor quantum dots is the main topic of this thesis.

Chapter 2

Mesoscopic physics

The terms macroscopic and microscopic traditionally signify the part of the world that is directly accessible to the naked eye (e.g., a flat wall), and the part of the world which is to small to see unaided (e.g., the rough and weird surface of the flat wall in a scanning electron microscope). As the electronic industry has progressed from the macroscopic world of vacuum tubes towards the microscopic world of molecular electronics, the need to name an intermediate region has come about. This region is now labelled *mesoscopic*, where the prefix derives from the Greek word "*mesos*", which means 'in between'. Mesoscopic systems are small enough to require a quantum mechanical description but at the same time too big to be described in terms of individual atoms or molecules, thus 'in between' the macroscopic and the microscopic world.

The mesoscopic length scale is limited by a couple of characteristics lengths as larger systems will not behave quantum mechanically:

- The mean free path of the electrons.
- The phase-relaxation length, the distance after which the original phase of the electron is lost.

Depending on the material used, the temperature, etc., these lengths and the actual size of a mesoscopic system could vary from a few nanometres to several hundred micrometres [4].

This chapter introduces manufacturing techniques, classification and general concepts of low-dimensional and semiconductor systems.

2.1 Heterostructures

A heterostructure is a semiconductor composed of more than one material. By mixing layers of materials with different bandgaps, i.e. *band-engineering*, it is possible to restrict electron movement to the interface (the heterojunction) between the materials. This is typically the first step in the fabrication of low-dimensional devices. Since any defects at the interface will impair electron

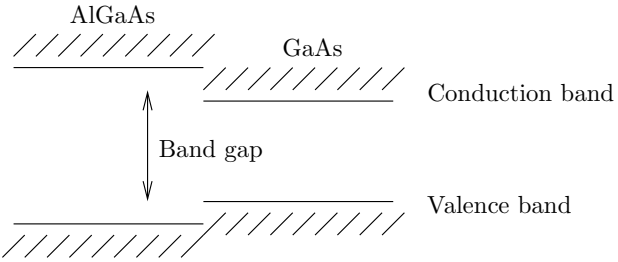

Figure 2.1: Bandgap for AlGaAs (left) and GaAs (right) schematically. For these materials their corresponding bandgap results in a *straddling alignment*, i.e., the smaller bandgap in GaAs is entirely enclosed by the larger bandgap in AlGaAs.

mobility through *surface-roughness scattering*, successful heterostructure fabrication techniques must yield a very fine and smooth interface. Two of the most common growth methods are *molecular beam epitaxy* (MBE) and *metal-organic chemical vapour deposition* (MOCVD). In MBE, a beam of molecules is directed towards the substrate in an ultra high vacuum chamber, while in MOCVD a gas mixture of the desired molecules are kept at specific temperatures and pressures in order to promote growth on a substrate. Both these techniques allow good control of layer thickness and keep impurities low at the interface.

In addition to the problem with surface-roughness, a mechanical stress due to the lattice constant mismatch between the heterostructure materials causes dislocations at the interface. This restricts the number of useful semiconductors to those with close/similar lattice constants. A common and suitable choice, because of good lattice constant match and bandgap alignment (see figure 2.1), is to grow $Al_xGa_{1-x}As$ (henceforth abbreviated AlGaAs, with the mixing factor x kept implicit) on top of a GaAs substrate. The position and relative size of the bandgap in a GaAs-AlGaAs heterostructure is schematically shown in figure 2.1. At room temperature the bandgap for GaAs is 1.424eV[19], while the bandgap in AlGaAs depends on the mixing factor x and can be approximated by the formula[19]

$$E_g(x) = 1.424 + 1.429x - 0.14x^2[\text{eV}] \qquad 0 < x < 0.44^1, \tag{2.1}$$

i.e., it varies between 1.424-2.026eV.

2.2 Two-dimensional systems

Working with the GaAs-AlGaAs mentioned above, a two-dimensional electron system is typically created by n-doping the AlGaAs in an heterostructure (fi-

[1]For larger x the smallest bandgap in AlGaAs is indirect.

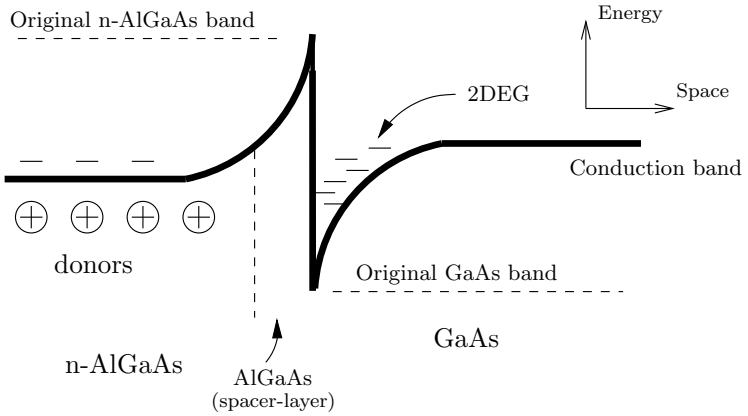

Figure 2.2: Two-dimensional electron gas seen along the confining dimension.

gure 2.2 or the left panel of figure 2.4). Some of the electrons added will eventually migrate into the GaAs. These electrons will still be attracted by the positive donors in the AlGaAs, but be unable to go back across the heterojunction because of the conduction band discontinuity. Squeezed in between the discontinuity and the donor potential, they are trapped in a narrow potential well (see figure 2.2). Similar to the schoolbook example of the quantum well, their energy component in this dimension will be quantised. Because the potential well is very narrow (typically 10nm[6]), the available energy states will be sparsely spaced, and at sufficiently low temperatures *all* electrons will be in the same (the lowest) energy state with respect to motion perpendicular to the interface. I.e., electrons are free to move in the plane parallel to the heterojunction, but restricted to the same (lowest) energy state in the third dimension. In this sense we talk about a two-dimensional electron gas (2DEG).

To put the donors only in the AlGaAs layer (*remote* or *modular* doping) prevents the electrons at the heterojunction to scatter against the positive donors. Usually an additional layer of undoped AlGaAs is grown at the interface as a spacer layer. This will, at the expense of high electron density, further shield the electrons from scattering. Densities in 2DEGs typically varies between $1 - 5 \times 10^{15}\mathrm{m}^{-1}$ though values as low as $5 \times 10^{13}\mathrm{m}^{-1}$ has been reported[13].

2.2.1 Density of States

A simple but yet powerful characterisation of a system is given by its density of states (DOS), $N(E)$, where $N(E)dE$ is defined as the number of states in the energy interval $E \to E + dE$. For free electrons it is possible to determine the 2-dimensional DOS, $N_{2D}(E)$, exactly. This is done by considering electrons

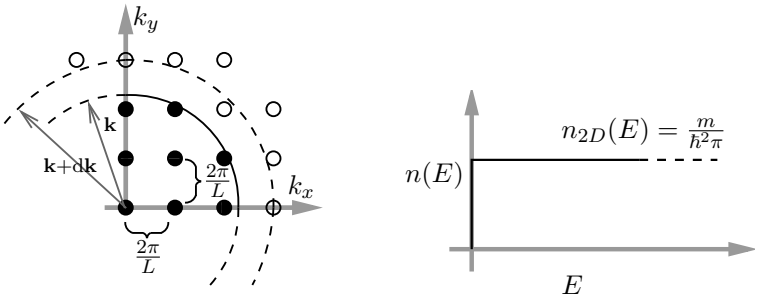

(a) 2D **k**-space (b) 2D density of states

Figure 2.3: **(a)** Occupied and unoccupied (filled/empty circles) states in 2D **k**-space. **(b)** The two-dimensional density of states, $n_{2D}(E)$.

put in a square of area L^2 and letting $L \to \infty$. With periodic boundary conditions the solutions are travelling waves,

$$\phi(\mathbf{r}) = e^{i\mathbf{k}\cdot\mathbf{r}} = e^{i(k_x x + k_y y)}, \tag{2.2}$$

where

$$\mathbf{k} = (k_x, k_y) = \left(\frac{2\pi m}{L_x}, \frac{2\pi n}{L_y}\right) = \left(\frac{2\pi m}{L}, \frac{2\pi n}{L}\right) \qquad m, n = 0, \pm 1, \pm 2 \ldots . \tag{2.3}$$

Plotting these states in the 2-dimensional k-space, figure 2.3**a**, we recognise that a unit cell has the area $\left(\frac{2\pi}{L}\right)^2$, hence the density of states is

$$N_{2D}(\mathbf{k}) = 2\left(\frac{(2\pi)^2}{L^2}\right)^{-1} = \frac{L^2}{2\pi^2} \tag{2.4}$$

where a factor two is added to include spin. Defining the density of states per unit area,

$$n_{2D}(\mathbf{k}) = \frac{N_{2D}(\mathbf{k})}{L^2} = \frac{1}{2\pi^2}, \tag{2.5}$$

we get a quantity that is defined as $L \to \infty$. In order to change variable from $n_{2D}(\mathbf{k})$ to $n_{2D}(E)$, we look at the annular area described by $\mathbf{k}$ and $\mathbf{k}$+d$\mathbf{k}$ in figure 2.3**a**. This area is approximated by $2\pi k dk$ and, thus, contains $n_{2D}(k)2\pi k dk$ states. The number of states must of course be the same whether we express it in terms of wave vector $\mathbf{k}$ or energy E, i.e.,

$$n_{2D}(E)dE = n_{2D}(E)\frac{dE}{dk}dk = 2\pi k n_{2D}(k)dk = 2\pi k \frac{1}{2\pi^2}dk \tag{2.6}$$

$$\Leftrightarrow n_{2D}(E) = \frac{k}{\pi}\left(\frac{dE}{dk}\right)^{-1}. \tag{2.7}$$

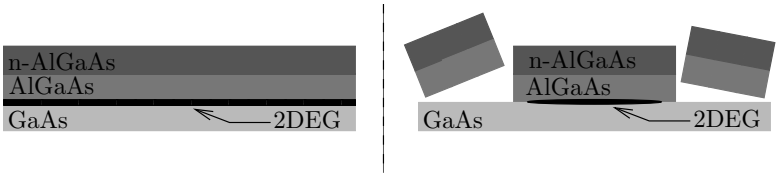

Figure 2.4: **Left:** 2DEG in AlGaAs-GaAs heterostructure. **Right:** Etching away the AlGaAs everywhere but in a narrow stripe results in a one-dimensional quantum wire beneath the remaining AlGaAs.

For free electrons, with

$$E(k) = \frac{\hbar^2 k^2}{2m}, \qquad \text{where } k = |\mathbf{k}| \tag{2.8}$$

we finally arrive at

$$n_{2D}(E) = \frac{m}{\hbar^2 \pi}, \tag{2.9}$$

shown in figure 2.3**b**.

2.3 One-dimensional systems

There are several techniques to further restrict the 2DEG in order to get an essentially one-dimensional system – a so called quantum wire. Two common approaches are chemical etching, or to put metallic gates on top of the sample.

Etching

By etching away part of the top dopant layer, the electron gas is located to the area beneath the remaining dopant as schematically illustrated in figure 2.4.

Metallic gates

A second alternative is to deploy metallic gates on top of the surface as shown in figure 2.5. By applying a negative voltage to the gates, the 2DEG will be depleted beneath them. This technique allows experimenters to control the approximate size of the system by changing the applied potential during the experiment.

2.3.1 Density of States in one dimension

Just as in the two-dimensional case, an exact expression for the the density of states for free electrons can be found. The derivation is similar – starting with periodic boundary conditions in a one-dimensional box of size L, the solutions

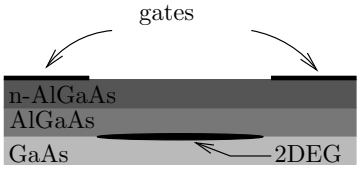

Figure 2.5: A negative potential applied to lithographically deployed gates shuns away the electrons away from the area beneath the gates.

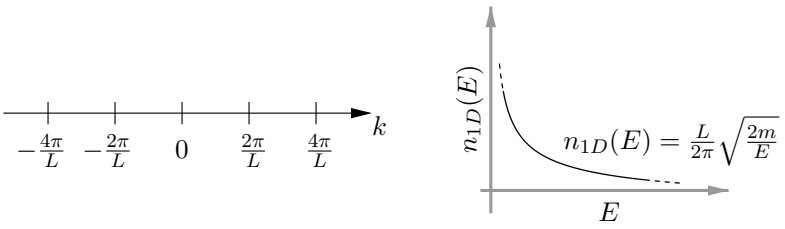

(a) 1D '**k**-space' (b) 1D density of states

Figure 2.6: **(a)** Available states in one dimensional 'k-space' (at $k{=}\pm\frac{2\pi n}{L}$). **(b)** The one-dimensional density of states, $n_{1D}(E)$.

are

$$\phi(x) = e^{ikx}, \qquad \text{where } k = \frac{2\pi n}{L},\ n = 0, \pm1, \pm2, \ldots \tag{2.10}$$

Plotting the allowed states along the x-axis (figure 2.6**a**) we see that a unit length is $\frac{2\pi}{L}$. Adding a factor two to account for both spin directions, the number of states, $N_{1D}(k)dk$ in a small interval dk is,

$$N_{1D}(k)dk = 2\frac{L}{2\pi}dk = \frac{L}{\pi}dk. \tag{2.11}$$

Keeping in mind that each energy E corresponds to two k's ($\pm k$), we equate the number of states expressed in terms of wave-vector k and energy E,

$$2N_{1D}(k)dk = N_{1D}(E)dE \tag{2.12}$$

$$\Leftrightarrow \qquad 2N_{1D}(k)dk = N_{1D}(E)\frac{dE}{dk}dk \tag{2.13}$$

$$\underset{\textbf{eq. (2.8)}}{\Leftrightarrow} \qquad 2N_{1D}(k)dk = N_{1D}(E)\frac{\hbar^2 k}{m}dk \tag{2.14}$$

$$\underset{\textbf{eq. (2.11)}}{\Leftrightarrow} \qquad 2\frac{L}{\pi}dk = N_{1D}(E)\frac{\hbar^2 k}{m}dk \tag{2.15}$$

$$\Leftrightarrow \qquad \frac{2mL}{\pi\hbar^2 k} = N_{1D}(E) \tag{2.16}$$

$$\underset{\text{eq. (2.8)}}{\Leftrightarrow} \qquad \frac{L}{\hbar\pi}\sqrt{\frac{2m}{E}} = N_{1D}(E) \tag{2.17}$$

$$\Leftrightarrow \qquad \frac{1}{\hbar\pi}\sqrt{\frac{2m}{E}} = \frac{N_{1D}(E)}{L} = n_{1D}(E). \tag{2.18}$$

$n_{1D}(E)$, shown in figure 2.6, is defined as the density of states per unit length, valid as $L \to \infty$.

2.3.2 Subbands in one dimesion

The transversal confinement in a one-dimensional system results in a quantisation of energies in this dimension. Denoting the confining potential $U(y)$ (i.e., electrons are free along the x-axis), the Schrödinger equation

$$-\frac{\hbar^2}{2m}\left(\frac{\partial^2}{\partial x^2} + \frac{\partial^2}{\partial y^2} + U(y)\right)\Psi(x,y) = E\Psi(x,y), \tag{2.19}$$

can, by introducing $\Psi(x,y) = \psi(x)\phi(y)$, be separated into

$$-\frac{\hbar^2}{2m}\frac{d^2}{dx^2}\psi(x) = E_x\psi(x) \tag{2.20}$$

$$-\frac{\hbar^2}{2m}\left(\frac{d^2}{dy^2} + U(y)\right)\phi(y) = E_y\phi(y). \tag{2.21}$$

In the simple case of a hard wall potential $U(y)$,

$$U(y) = \begin{cases} 0, & 0 < y < w \\ \infty, & y < 0 \cup w < y, \end{cases} \tag{2.22}$$

eq. (2.20) and (2.21) yields the solutions

$$\Psi_n(x,y) = \psi(x)\phi_n(y) = e^{ik_x x}\sin\left(\frac{\pi n y}{w}\right) \tag{2.23}$$

and eigenenergies

$$E = E_x + E_{y,n} = \frac{\hbar^2}{2m}\left(k_x^2 + \left(\frac{\pi n}{w}\right)^2\right) = \frac{\hbar^2}{2m}\left(k_\parallel^2 + \pi^2 k_\perp^2\right). \tag{2.24}$$

The total energy E is the sum of a continuous part E_x, and a discreet part $E_{y,n}$ with corresponding continuous ($k_\parallel$) and and discrete ($k_\perp$) wave-vectors. Hence, the energy dispersion relation, $E(k) = E(k_\parallel + k_\perp) \sim k_\parallel^2 + k_\perp^2$, consists of subbands, as depicted in figure 2.7.

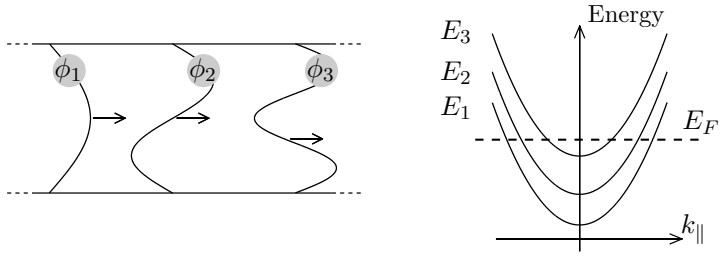

(a) Wave functions for the 3 lowest prop. states

(b) Subbands for 3 lowest states

Figure 2.7: **(a)** The three lowest propagating nodes, $\phi_i(y)$, in a hard wall potential quantum wire. **(b)** Corresponding subbands to $\phi_1(y)$–$\phi_3(y)$ seen in (a). The Fermi energy is indicated by E_F.

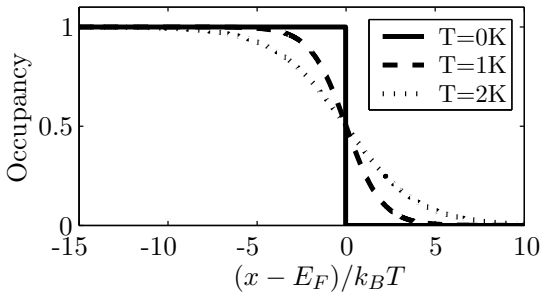

Figure 2.8: Fermi-Dirac distribution for the temperatures T=0,1,2 Kelvin.

2.4 Fermi-Dirac distribution

At temperature T=0K (or for free electrons), the electrons in the 2DEG will occupy the states with lowest possible energy according to the Pauli principle, in figure 2.3**a** shown as a circle of occupied states. The vector $\mathbf{k}_F$, which describes the radius of this circle, is called the Fermi wave vector and the corresponding energy, $E_F = \frac{\hbar^2 k_F^2}{2m}$, the Fermi energy (from now on subscripted k_F and E_F respectively). The total electron density, $n_e(\mathbf{r})$ can be found by integrating the DOS up to E_F,

$$n_e(\mathbf{r}) = \int_{-\infty}^{E_F} \underbrace{n(E, \mathbf{r})}_{\text{DOS}} dE. \tag{2.25}$$

However, if T>0K, some of the electrons below the Fermi energy becomes excited and it is no longer enough to know the DOS in order to find the

electron density, we also need the distribution of occupied states. This is given by the Fermi-Dirac distribution (figure 2.8),

$$f_{FD}(x, E_F, T) = \frac{1}{1 + e^{\frac{x - E_F}{k_B T}}}, \tag{2.26}$$

where k_B is the Boltzmann constant. For a specific Fermi energy (E_F) and temperature (T), the electron density is now given by

$$n_e(\mathbf{r}, E_F, T) = \int_{-\infty}^{\infty} \underbrace{n(E, \mathbf{r})}_{\text{DOS}} \underbrace{f_{FD}(E, E_F, T)}_{\text{F-Ddist.}} dE. \tag{2.27}$$

Chapter 3

Transport in mesoscopic systems

Understanding transport is central to the study of mesoscopic systems. Often transport characteristics work as a flexible tool to probe the electron states inside a system – well-known examples are the Kondo effect[17] and the 0.7-anomaly[9]. This chapter introduces some basics of *ballistic* transport in mesoscopic systems, that is, systems where electrons pass through the conductor without scattering and remain phase coherent. In brief, we will start by deriving the Landauer formula which describes transport for a system with only two leads connected. This is then generalised within the Büttiker formalism to handle an arbitrary number of leads. A key characteristic for the quantum conductance in these expressions is the transmission probability $T_{n,\beta\leftarrow m,\alpha}$, i.e., the probability for an electron in mode α and lead m to end up in another mode β and lead n. Finally we will look at effects on transport when a perpendicular magnetic field is applied.

3.1 Landauer formula

3.1.1 Single propagating mode

For simplicity we start with the case of a single propagating mode (see figure 2.7**a**), i.e., where only the lowest subband in both the left and right lead is occupied. Figure 3.1 shows electrons surrounding a barrier in a 1-dimensional system with some bias eV applied. Though in principle, the Fermi energy is only defined at equilibrium, we will assume this bias to be small enough to yield a near-equilibrium electron distribution that is characterised by a quasi-Fermi level, E_{Fl} and E_{Fr} respectively. To find an explicit expression for the net current across the barrier due to the bias we first consider the electrons approaching the barrier from the left. In an infinitesimal momentum interval

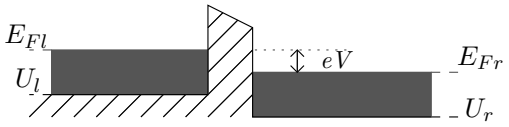

Figure 3.1: Schematic view of a 1D barrier surrounded by electrons. A small bias eV shifts the (quasi-)Fermi levels in left (E_{Fl}) and right (E_{Fr}) lead.

dk around k, the transmitted current is

$$I_l(k)dk = 2en_{1D}(k)v(k)T_{r\leftarrow l}(k)f\big(E(k), E_{Fl}\big)dk \tag{3.1}$$

where a factor 2 is added to include spin, e the electron charge, $n_{1D}(k)$ is the one-dimensional density of states, $v(k)$ the velocity of the electrons, $T_{r\leftarrow l}(k)$ the probability that an electron passes the barrier and $f\big(E(k), E_{Fl}\big)$ the Fermi-Dirac distribution. Using eq. (2.18) for the 1D-DOS and integrating both sides yields

$$\begin{aligned} I_l = \int_0^\infty 2e\frac{1}{2\pi}v(k)T_{r\leftarrow l}(k)f\big(E(k), E_{Fl}\big)dk = \Big\backslash dk = \frac{dk}{dE}dE\Big\backslash \\ = \frac{2e}{2\pi}\int_0^\infty v(E)T_{r\leftarrow l}(E)f\big(E, E_{Fl}\big)\frac{dk}{dE}dE. \end{aligned} \tag{3.2}$$

Recognising the group velocity as $v = \frac{d\omega}{dk} = \frac{1}{\hbar}\frac{dE}{dk}$ and integrating from the bottom of the left lead brings

$$\begin{aligned} I_l = \frac{2e}{2\pi}\int_{U_l}^\infty v(E)T_{r\leftarrow l}(E)f\big(E, E_{Fl}\big)\frac{1}{\hbar v(E)}dE \\ = \frac{2e}{h}\int_{U_l}^\infty T_{r\leftarrow l}(E)f\big(E, E_{Fl}\big)dE. \end{aligned} \tag{3.3}$$

There is, except for the different Fermi level and opposite direction of flow, a similar current I_r from the right to left lead. If the bias is small, the reciprocity relation $T_{l\leftarrow r}(E)$=$T_{r\leftarrow l}(E)$ holds (see e.g. [5]), and we can skip the indices on the transmission coefficient. The net current becomes

$$I = I_l + I_r = \frac{2e}{h}\int_{U_l}^\infty T(E)\Big[f\big(E, E_{Fl}\big) - f\big(E, E_{Fr}\big)\Big]dE. \tag{3.4}$$

In the case of very low bias eV, i.e., in the *linear response regime*, the Fermi-Dirac functions in eq. (3.4) can be Taylor expanded around E_F=$\frac{1}{2}(E_{Fl}+E_{Fr})$ according to

$$f(E, E_{Fl}) - f(E, E_{Fl}) = f(E, E_F + \frac{1}{2}eV) - f(E, E_F - \frac{1}{2}eV)$$

$$= eV\frac{\partial f(E,E_F)}{\partial E_F} + \bigcirc\left((eV)^2\right) \approx -eV\frac{\partial f(E,E_F)}{\partial E}, \quad (3.5)$$

resulting in

$$I = \frac{2e}{h}\int_{U_l}^{\infty} T(E)\left(-eV\frac{\partial f(E,E_F)}{\partial E}\right)dE \quad (3.6)$$

$$\Leftrightarrow$$

$$G = \frac{I}{V} = \frac{2e^2}{h}\int_{U_l}^{\infty} T(E)\left(-\frac{\partial f(E,E_F)}{\partial E}\right)dE. \quad (3.7)$$

At very low temperatures in the linear response regime, $-\frac{\partial f}{\partial E}$ is replaced by the Dirac delta function $\delta(E - E_F)$ and evaluating the integral in eq. (3.7) gives the famous Landauer formula for quantum conductance

$$G = \frac{I}{V} = \frac{2e^2}{h}T(E_F). \quad (3.8)$$

3.1.2 Several propagation modes

The result in eq. (3.8) above is readily extended to the case of several propagating modes in the leads. An electron incoming towards a scatterer in a specific mode α might be transmitted to some mode β in the opposite lead or reflected to some mode β in the same lead. By summing over all possible modes the total conductance is found as

$$G = \frac{2e^2}{h}\sum_{\alpha,\beta} T_{\beta\leftarrow\alpha}. \quad (3.9)$$

3.2 Büttiker formalism

Büttiker formalism describes transport in systems with more than two leads. A typical example is the three lead system where a net current flows between two leads (*current probes*), and the third lead is used to measure the potential (*voltage probe*). We will assume fairly low temperature and bias. In this limit the Fermi-Dirac functions in eq. (3.4) may be replaced by step functions (fig. 2.8),

$$I = \frac{2e}{h}\int_{U_l}^{\infty} T(E)\Big[\Theta\big(E_{Fl} - E\big) - \Theta\big(E_{Fr} - E\big)\Big]dE$$

$$= \frac{2e}{h}\int_{E_{Fr}}^{E_{Fl}} T(E)dE. \quad (3.10)$$

With low bias we assume $T(E)$ to be constant in the interval $E_{Fr} < E < E_{Fl}$, thus the integral in eq. (3.10) evaluates to

$$I = \frac{2e}{h}T \times (E_{Fl} - E_{Fr}). \quad (3.11)$$

We now consider a system connected to an arbitrary number of leads (indexed by m and n) and propagating modes (α and β). I_m denotes the total net current in lead m. It is the sum of the net incident current I_{mm} ($I_{incoming} - I_{reflected}$) and the current injected from all other leads, $\sum_{n\neq m} I_{m\leftarrow n}$. With the lowest quasi-Fermi level in all leads denoted E_0 we can write

$$I_{m\leftarrow n} = -\frac{2e}{h}\sum_{n\neq m}\sum_{\alpha,\beta} T_{m,\alpha\leftarrow n,\beta}\times(E_n - E_0). \tag{3.12}$$

The minus sign indicates a current away from the system and $T_{m,\alpha\leftarrow n,\beta}$ is the transmission probability from lead n–mode β to lead m–mode α. We will abbreviate this by the notation

$$\bar{T}_{m\leftarrow n} = \sum_{\alpha,\beta} T_{m,\alpha\leftarrow n,\beta}, \tag{3.13}$$

and in a similar way

$$\bar{R}_m = \sum_{\alpha,\beta} R_{m,\alpha\leftarrow m,\beta} \tag{3.14}$$

for the reflection $R_{m,\alpha\leftarrow m,\beta}$ from from mode β to α in lead m. Lead m carries N_m propagating modes hence the net incident current in lead m is

$$I_{mm} = \frac{2e}{h}\left(N_m - \bar{R}_m\right)(E_m - E_0). \tag{3.15}$$

Furthermore, conservation of flux requires that

$$N_m = \bar{R}_m + \sum_{m\neq n}\bar{T}_{n\leftarrow m} = \bar{R}_m + \sum_{n\neq m}\bar{T}_{m\leftarrow n} \tag{3.16}$$

where the last equality follows from the sum rule derived in eq. (3.30)–(3.35). The total current in lead m can be written as

$$I_m = I_{mm} + I_{m\leftarrow n} = \frac{2e}{h}\left(N_m - \bar{R}_m\right)(E_m - E_0) - \frac{2e}{h}\sum_{n\neq m}\bar{T}_{m\leftarrow n}(E_n - E_0) \tag{3.17}$$

$$= \frac{2e}{h}\sum_{n\neq m}\bar{T}_{m\leftarrow n}(E_m - E_0) - \frac{2e}{h}\sum_{n\neq m}\bar{T}_{m\leftarrow n}(E_n - E_0) \tag{3.18}$$

$$= \frac{2e}{h}\sum_{n\neq m}\left(\bar{T}_{m\leftarrow n}E_m - \bar{T}_{m\leftarrow n}E_n\right), \tag{3.19}$$

where eq. (3.16) has been used in the second step. Noting that $E_m = eV_m$ we finally get

$$I_m = \frac{2e^2}{h}\sum_{n\neq m}\bar{T}_{m\leftarrow n}\left(V_m - V_n\right). \tag{3.20}$$

The currents in a multi-lead system are then found from solving the system of equations defined by equation (3.20).

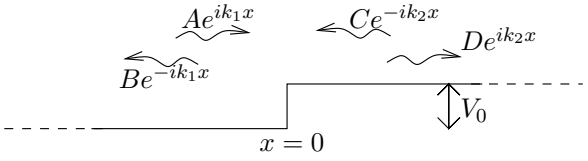

Figure 3.2: Incoming and outgoing electrons at a potential step.

3.3 Matching wave functions

The solution to the Schrödinger eq. for electrons with energy $E > V_0$ in the potential step shown in fig. 3.2 is

$$\Psi(x) = \begin{cases} Ae^{ik_1x} + Be^{-ik_1x} & x < 0 \\ Ce^{-ik_2x} + De^{ik_2x} & x > 0. \end{cases} \tag{3.21}$$

The requirement that the wave function and its derivative is continuous at $x = 0$ yields the system of equations

$$A + B = C + D \tag{3.22}$$
$$k_1(A - B) = k_2(D - C). \tag{3.23}$$

Solving for the outgoing amplitudes, B and D, results in

$$\begin{pmatrix} B \\ D \end{pmatrix} = \frac{1}{k_1 + k_2} \begin{pmatrix} k_1 - k_2 & 2k_1 \\ 2k_1 & k_2 - k_1 \end{pmatrix} \begin{pmatrix} A \\ C \end{pmatrix}. \tag{3.24}$$

E.g., for a free electron incoming from the left with unit amplitude ($A = 1$, $C = 0$), the transmitted amplitude ($D = t_{2\leftarrow1}$) becomes

$$t_{2\leftarrow1} = \frac{2k_1}{k_1 + k_2}, \tag{3.25}$$

and the reflected amplitude ($B = r_{1\leftarrow1}$)

$$r_{1\leftarrow1} = \frac{k_1 - k_2}{k_1 + k_2}. \tag{3.26}$$

Because the velocities in the left and right lead may differ, the flux transmission coefficient becomes

$$T_{2\leftarrow1}(k_1, k_2) = \frac{v_2(k_2)}{v_1(k_1)} |t_{2\leftarrow1}|^2, \tag{3.27}$$

where v_2 and v_1 are the group velocities for the electron.

3.3.1 S-matrix formalism

The matrix equation (3.24) above relates the amplitude of the outgoing electrons to the amplitude of the incoming electrons. The current into the system for mode i is given by $I_i = -v_i(k)|A_i(k)|^2$ where $v_i(k)$ is the group velocity and $A_i(k)$ the amplitude. It is convenient to define the *current amplitude*, by

$$\begin{aligned} a_i(k) =& A_i(k)\sqrt{-v(k)} && \text{(current amplitude for incoming mode } i\text{)} \\ b_i(k) =& B_i(k)\sqrt{v(k)} && \text{(current amplitude of outgoing mode } i\text{),} \end{aligned}$$

such that the current carried by mode i simply is $I_i = |a_i(k)|^2$. We now generalise eq. (3.24) to handle an arbitrary system by defining the S-matrix (scattering matrix)[4],

$$\bar{\mathbf{b}} = \mathsf{S}\bar{\mathbf{a}}, \tag{3.28}$$

which, for each energy E, relates the incident current amplitudes $\mathbf{a} = (a_1, a_2, \ldots, a_n)$ to the outgoing current amplitudes $\mathbf{b} = (b_1, b_2, \ldots, b_n)$. The transmission probability now equals

$$T_{m\leftarrow n}(E) = |s_{mn}|^2, \tag{3.29}$$

where s_{mn} is a matrix element in the S-matrix. Using S-matrices we can prove the sum-rule used in eq. (3.16). Current conservation requires that

$$I_{in} = e\sum_i |a_i|^2 = e\sum_i |b_i|^2 = I_{out} \tag{3.30}$$

or in matrix notation

$$\begin{aligned} & \bar{\mathbf{a}}^\dagger\bar{\mathbf{a}} = \bar{\mathbf{b}}^\dagger\bar{\mathbf{b}} && (3.31) \\ \overset{\text{eq. (3.28)}}{\Leftrightarrow} \quad & \bar{\mathbf{a}}^\dagger\bar{\mathbf{a}} = (\mathsf{S}\bar{\mathbf{a}})^\dagger\,\mathsf{S}\bar{\mathbf{a}} && (3.32) \\ \Leftrightarrow \quad & \bar{\mathbf{a}}^\dagger\bar{\mathbf{a}} = \bar{\mathbf{a}}^\dagger\mathsf{S}^\dagger\mathsf{S}\bar{\mathbf{a}} && (3.33) \\ \Rightarrow \quad & \mathsf{S}^\dagger\mathsf{S} = \mathrm{I} = \mathsf{S}\mathsf{S}^\dagger, && (3.34) \end{aligned}$$

i.e., S is unitary and we can write

$$\sum_m T_{m\leftarrow n} = \sum_m |s_{mn}|^2 = 1 = \sum_m |s_{nm}|^2 = \sum_m T_{n\leftarrow m}. \tag{3.35}$$

3.4 Magnetic fields

Magnetic field is usually incorporated into the Hamiltonian through a vector potential $\mathbf{A}$ defined by the equation

$$\mathbf{B} = \nabla \times \mathbf{A} \tag{3.36}$$

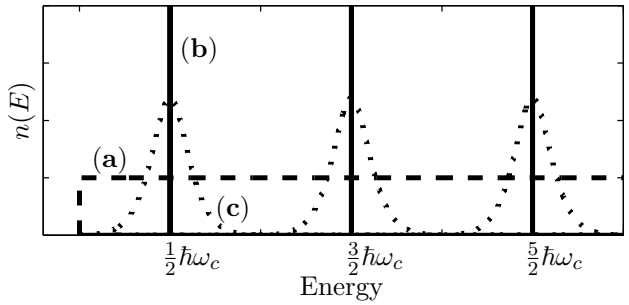

Figure 3.3: (**a**)–dashed line: 2D density of states with B=0T. (**b**)–solid line: Ideal 2D density of states in a magnetic field. (**c**)–dotted line: Broadened 2D density of states in a magnetic field.

as

$$H = \frac{1}{2m}\left(-i\hbar\nabla + e\mathbf{A}\right)^2 + V. \tag{3.37}$$

Since $\nabla \times \nabla\xi = 0$ for any function ξ, there is a possibility to choose different *gauges*, $\mathbf{A}\rightarrow\mathbf{A}+\nabla\xi$, without changing the physical properties of the system. Some common choices for a magnetic field B$\hat{\mathbf{z}}$ is Landau gauge $\mathbf{A}$=$(-By,0,0)$ or $\mathbf{A}$=$(0,Bx,0)$, and the circular symmetric gauge $\mathbf{A}$=$\frac{1}{2}(-By, Bx,0)$. We will now consider $\mathbf{A}$=$(0,Bx,0)$, and the Schrödinger equation for a 2DEG becomes

$$H\Psi = \left(-\frac{\hbar}{2m}\nabla^2_{x,y} - \frac{ie\hbar Bx}{m}\frac{\partial}{\partial y} + \frac{(eBx)^2}{2m}\right)\Psi(x,y) = E\Psi(x,y). \tag{3.38}$$

Trying a solution in the form $\Psi(x,y) = u(x)e^{iky}$ we end up with an equation only in x,

$$\left(-\frac{\hbar^2}{2m}\frac{d^2}{dx^2} + \frac{1}{2m}\left(\hbar k + eBx\right)^2\right)u(x) = \epsilon u(x) \tag{3.39}$$

$$\Leftrightarrow \quad \left(-\frac{\hbar^2}{2m}\frac{d^2}{dx^2} + \frac{m\omega_c^2}{2}\left(\frac{\hbar k}{eB} + x\right)^2\right)u(x) = \epsilon u(x) \tag{3.40}$$

with $\omega_c^2 = \frac{eB}{m}$ being the cyclotron frequency. This is the Schrödinger equation for a harmonic oscillator so we can write down the eigenenergies as

$$\epsilon_{n,k} = (n - \frac{1}{2})\hbar\omega_c, \quad n = 1, 2, 3, \ldots \tag{3.41}$$

The energies in eq. (3.41) are independent of k, hence the density of states – which for zero magnetic field is constant (eq. (2.9) or fig. 3.3) – now collapses to very narrow stripes, equidistantly located as shown in figure 3.3. These collapsed states are called Landau levels and contain all the degenerate states with the same k. In an actual system they are broadened due to scattering.

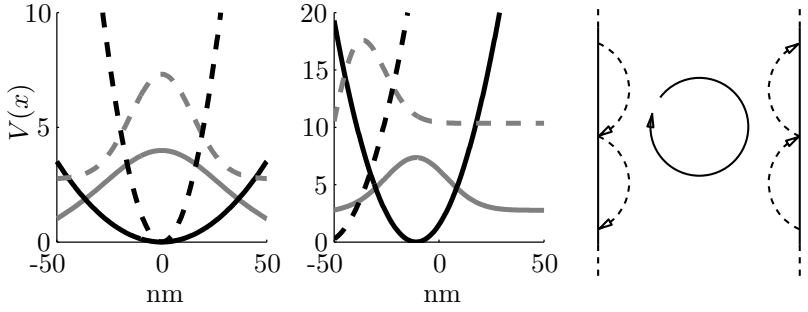

Figure 3.4: **Left:** Potentials (black) and wave functions (gray) for B=1T (solid lines) and $B = 3T$ (dashed lines) in a quantum wire, k=0. **Middle:** Potentials (black) and wave functions (gray) for k=0.05nm^{-1} (solid lines) and k=0.25nm^{-1} (dashed lines) in a quantum wire, $B = 3T$. **Right:** Classical skipping orbits in a straight quantum wire.

Next we consider a hard wall potential electron wave-guide of the width L, oriented along the y-axis. Trying the same solution as above, $\Psi(x, y) = u(x)e^{iky}$, we arrive at

$$\left(-\frac{\hbar^2}{2m}\frac{d^2}{dx^2} + \frac{m\omega_c^2}{2}\left(\frac{\hbar k}{eB} + x\right)^2 + V(x)\right)u(x) = \epsilon u(x) \tag{3.42}$$

where the only difference from eq. (3.40) is the confining potential $V(x)$,

$$V(x) = \begin{cases} 0 & |x| \leq \frac{L}{2} \\ \infty & |x| > \frac{L}{2} \end{cases}. \tag{3.43}$$

This equation do not have an analytical solution but we may still draw some qualitative conclusions from eq. (3.42). The electrons are confined by the hard wall potential $V(x)$ and the parabolic potential which depends on k and B. With k=0, the parabolic potential is determined only by the magnetic field B (through w_c), and an increasing magnetic field will steepen the potential thereby confining the electrons to the middle of the wire as shown in the leftmost panel of figure 3.4. For $|k|$ >0 the vertex of the parabola is displaced, and for large $|k|$'s the wave function is squeezed against the hard wall confinement (middle panel of figure 3.4). Hence, currents in this system are carried along the edges of the wire by these "edge states". The classical equivalence to this is the so called skipping orbits shown in the rightmost panel of the same figure. Due to the Lorentz force, an electron in a perpendicular magnetic field moves in a circle and do not contribute to any net current. However, along the edges of the wire electrons will bounce off the walls, resulting in a current in both directions.

Chapter 4

Density Functional Theory

Some years after the Schrödinger equation and the basics of quantum mechanics had been formulated, Paul Dirac commented that

> The underlying physical laws necessary for the mathematical theory of a large part of physics and the whole of chemistry are thus completely known, and the difficulty is only that the exact application of these laws leads to equations much too complicated to be soluble.[7]

The results from quantum mechanics were impressive already by 1929, but there was also an awareness of the huge computational effort needed to solve some (most) problems. Today, one of the most successful approaches to electronic structure calculations is the Density Functional Theory (DFT), where the many-body wave function $\Psi(\mathbf{r}_1, \mathbf{r}_2, \ldots)$ from the Schrödinger equation is replaced by the far simpler electron density, $n(\mathbf{r})$. This chapter gives a brief summary of DFT.

4.1 What's the problem?

The properties of a (stationary) N-electron system can be found by solving the (time-independent) Schrödinger equation

$$\hat{H}\Psi = \left(-\sum_i \frac{\hbar^2}{2m}\nabla_i^2 + \frac{1}{2}\sum_{i\neq i'} \frac{e^2}{|r_i - r_{i'}|} + v_{ext}(\mathbf{r}) \right) \Psi = E\Psi. \tag{4.1}$$

$\Psi{=}\Psi(\mathbf{r_1}, \mathbf{r_2}, \ldots, \mathbf{r_N})$ is the N-electron wave function in three dimensions, the terms in the brackets are the kinetic energy for the i:th electron, the electron-electron interaction and finally the external potential $v_{ext}(\mathbf{r})$. Because of the middle term in eq. (4.1) the coordinates $\mathbf{r}_1, \mathbf{r}_2, \ldots, \mathbf{r}_N$ are coupled and a direct solution for increasing N is a very difficult many-body problem. However, if we are only interested in the ground state of the system, another approach to

eq. (4.1) is available through the *Rayleigh-Ritz variational method*[3]. A trial wave function ϕ is introduced and an upper bound to the ground state energy E_0 is given by

$$E = E[\phi] = \frac{\langle\phi|\hat{H}|\phi\rangle}{\langle\phi|\phi\rangle} \geq E_0. \tag{4.2}$$

Equality holds when ϕ equals the true ground state wave function (Ψ_0). In practice, a number of parameters p_i may be introduced in the trial wave function and the ground state energy and wave functions can be found by minimising $E = E(p_1, p_2, \ldots, p_m)$ over the parameters p_i. The accuracy of the method depends on how closely the trial wave function ϕ resembles the actual wave function – the more parameters introduced, the better the result. However, as pointed out in for example[16], a rough estimate of the number of parameters needed for anything but very small systems is discouraging. If we introduce three parameters per spatial variable and consider a system of N=100 electrons, the total number of parameters (M_p) over which to perform the minimisation becomes

$$M_p = 3^{3N} = 3^{300} \sim 10^{143}! \tag{4.3}$$

Clearly this is not a feasible problem and is sometimes referred to as the *exponential wall*, since the size of the problem grows exponentially with the number of electrons.

4.2 Thomas-Fermi model

Equation (4.1) may be reformulated using the variational principle[20]

$$\delta E[\Psi] = 0, \tag{4.4}$$

i.e., solutions Ψ to the Schrödinger equation occurs at the extremum for the functional $E[\Psi]$. In order to have the wave function normalised, $\langle\Psi|\Psi\rangle = N$, a Lagrange multiplier E is introduced and we arrive at

$$\delta\left(\langle\Psi|\hat{H}|\Psi\rangle - E\left(\langle\Psi|\Psi\rangle - N\right)\right) = 0. \tag{4.5}$$

This is, however, only a rephrasing of the original Schrödinger equation (with the constraint $\langle\Psi|\Psi\rangle = N$) and by no means easier to solve. The idea in the Thomas-Fermi (TF) model is to assume that the ground state density,

$$n_0(\mathbf{r}) = \int \Psi_0(\mathbf{r}, \mathbf{r_2}, \ldots, \mathbf{r_N})\Psi_0^*(\mathbf{r}, \mathbf{r_2}, \ldots, \mathbf{r_N}) d\mathbf{r_2} d\mathbf{r_3} \ldots d\mathbf{r_N} \tag{4.6}$$

minimises the energy functional

$$E[n] = T[n] + U_{int}[n] + V_{ext}[n], \tag{4.7}$$

and thereby replace the wave function $\Psi(\mathbf{r}_1, \mathbf{r}_2, \ldots, \mathbf{r}_N)$ with the significantly simpler density $n(\mathbf{r})$. The first term $T[n]$ is the kinetic energy functional, in the original TF-model this was approximated by the expression for a uniform gas of non-interacting electrons. For the 2DEG we may find a similar expression from the 2D-density of states, $n_{2D}(\epsilon)=m/(\hbar^2\pi)$, given in eq. (2.9). The energy over some area L^2 is

$$\Delta E = \int_0^{\epsilon_F} \epsilon n_{2D}(\epsilon) L^2 d\epsilon = \frac{m}{\hbar^2\pi}\frac{\epsilon_F^2}{2}L^2, \tag{4.8}$$

where ϵ_F is the Fermi energy. At the same time the number of electrons in the area L^2 is

$$N = \int_0^{\epsilon_F} n_{2D}(\epsilon) L^2 d\epsilon = \frac{m}{\hbar^2}\epsilon_F L^2. \tag{4.9}$$

Thus,

$$\Delta E = \frac{m}{\hbar^2\pi}\frac{\epsilon_F^2}{2}L^2 = \frac{1}{2}e_F^2\frac{mL^2}{\hbar^2\pi} = \frac{1}{2}\left(\frac{\hbar^2\pi}{mL^2}N\right)^2\frac{mL^2}{\hbar^2\pi}$$
$$= \frac{1}{2}\frac{\hbar^2\pi}{m}\frac{N^2}{L^2} = \frac{\hbar^2\pi}{2m}n^2, \tag{4.10}$$

n being the electron density. The kinetic energy functional for a non-uniform 2DEG is now approximated by

$$T[n] \approx T_{TF}[n] = \frac{\hbar^2\pi}{2m}\int n(\mathbf{r})^2 d\mathbf{r} \tag{4.11}$$

where the integration is carried out over two dimensions. The second term in eq. (4.7) is the electron-electron interaction functional and was originally approximated by the classical Hartree energy,

$$U_{int}[n] \approx U_H[n] = \frac{e^2}{2}\int\int \frac{n(\mathbf{r_1})n(\mathbf{r_2})}{|\mathbf{r_1}-\mathbf{r_2}|}d\mathbf{r_1}d\mathbf{r_2}. \tag{4.12}$$

Finally, the last term is the energy due to interaction with some external potential $v_{ext}(\mathbf{r})$

$$V_{ext}[n] = e\int n(\mathbf{r})v_{ext}(\mathbf{r})d\mathbf{r}. \tag{4.13}$$

With the constraint

$$\int n(\mathbf{r})d\mathbf{r} = N \tag{4.14}$$

included through a Lagrange multiplier μ, which may be identified as the chemical potential, we arrive at

$$\delta\left[E[n] - \mu\left(e\int n(\mathbf{r})d\mathbf{r} - N\right)\right] = 0 \tag{4.15}$$

and consequently get the Euler-Lagrange equation

$$\mu = \frac{\delta E[n]}{\delta n} = \frac{\hbar^2\pi}{m}n(\mathbf{r}) + e^2\int\frac{n(\mathbf{r_1})}{|\mathbf{r}-\mathbf{r_1}|}d\mathbf{r_1} + ev_{ext}(\mathbf{r}), \tag{4.16}$$

which is the working equation in the Thomas-Fermi model.

4.3 Hohenberg-Kohn theorems

In 1964 Walter Kohn and Pierre Hohenberg proved two theorems[14], essential to any electronic state theory based on the electron density. The first theorem justifies the use of the electron density $n(\mathbf{r})$ as a basic variable as it uniquely defines an external potential and a wave function. The second theorem confirms the use of the energy variational principle for these densities, i.e., for a trial density $\tilde{n}(\mathbf{r}) > 0$, with the condition (4.14) fulfilled and $E[n]$ defined in eq. (4.7), it is true that

$$E_0 \leq E[\tilde{n}]. \tag{4.17}$$

The derivations below assume non-degeneracy but can be generalised to include degenerate cases[20].

4.3.1 The first HK-theorem

For an N electron system the Hamiltonian (and thereby the wave function Ψ) in eq. (4.1) is completely determined by the external potential $v_{ext}(\mathbf{r})$. N is directly obtained from the density through

$$N = \int n(\mathbf{r}) d\mathbf{r} \tag{4.18}$$

while the unique mapping between densities and external potentials are shown through a proof by contradiction. First assume there exists two different external potentials $v_{ext}(\mathbf{r})$ and $v'_{ext}(\mathbf{r})$[1], and thereby two different wave functions Ψ and Ψ', which yield the *same* electron density $n(\mathbf{r})$. Using eq. (4.2) we can write

$$\begin{aligned}\langle\Psi|\hat{H}|\Psi\rangle = E_0 < \langle\Psi'|\hat{H}|\Psi'\rangle &= \langle\Psi'|\hat{H}'|\Psi'\rangle + \langle\Psi'|\hat{H} - \hat{H}'|\Psi'\rangle \\ &= E'_0 - \int n(\mathbf{r}) \left(v_{ext}(\mathbf{r}) - v'_{ext}(\mathbf{r})\right) d\mathbf{r}\end{aligned} \tag{4.19}$$

and at the same time

$$\begin{aligned}\langle\Psi'|\hat{H}'|\Psi'\rangle = E'_0 < \langle\Psi|\hat{H}'|\Psi\rangle &= \langle\Psi|\hat{H}|\Psi\rangle + \langle\Psi|\hat{H}' - \hat{H}|\Psi\rangle \\ &= E_0 - \int n(\mathbf{r}) \left(v_{ext}(\mathbf{r}) - v'_{ext}(\mathbf{r})\right) d\mathbf{r}\end{aligned} \tag{4.20}$$

Adding equation (4.19) and (4.20) gives

$$E'_0 + E_0 < E'_0 + E_0 \tag{4.21}$$

and our assumption that different $v_{ext}(\mathbf{r})$ could yield the same density $n(\mathbf{r})$ is incorrect.

[1] differing more than $v_{ext}(\mathbf{r}) - v'_{ext}(\mathbf{r})$=constant

4.3.2 The second HK-theorem

From the first theorem we have that a density $n(\mathbf{r})$ uniquely determines a wave function Ψ, hence we can we define the functional

$$F[n(\mathbf{r})] = \langle \Psi | \hat{T} + \hat{U}_{int} | \Psi \rangle, \tag{4.22}$$

where $\hat{T}$ and $\hat{U}_{int}$ signify the kinetic energy and electron-electron interaction operator. According to the variational principle, the energy functional

$$E[\Psi] = \langle \Psi | \left(T + U_{int} \right) | \Psi \rangle + \int \Psi^* v_{ext}(\mathbf{r}) \Psi d\mathbf{r} \tag{4.23}$$

has a minimum for the ground state $\Psi{=}\Psi_0$. For any other $\Psi{=}\tilde{\Psi}$

$$E[\tilde{\Psi}] = \underbrace{F[\tilde{n}] + \int v_{ext}(\mathbf{r}) \tilde{n}(\mathbf{r}) d\mathbf{r}}_{=E[\tilde{n}]} \geq \underbrace{F[n_0] + \int v_{ext}(\mathbf{r}) n_0(\mathbf{r}) d\mathbf{r}}_{=E[n_0]} = E[\Psi_0] \tag{4.24}$$

and we arrive at (4.17).

The Hohenberg-Kohn theorems do not help us solve any specific many-body electron problem, however, they do show that there is no *principal* error in the Thomas-Fermi approach – only an error due to the approximations done for $T[n]$ and $U_{int}[n]$. With an exact expression for the functional $F[n] = T[n] + U_{int}[n]$ we could solve our problem exactly. Furthermore, since there is no reference to the external potential in $F[n]$, knowing this functional would allow us to solve any system. For this reason $F[n]$ is referred to as a *universal functional*.

4.4 The Kohn-Sham equations

Slightly over a year after the HK-theorems were published Walter Kohn and Lu Jeu Sham derived a set of equations, the Kohn-Sham equations, that made density functional calculations feasable[15]. They started by considering a system of *non-interacting* electrons moving in some effective potential $v_{eff}(\mathbf{r})$, which will be defined later. Because the system is non-interacting the ground state density $n(\mathbf{r})$ can be found by solving the single particle equation

$$\left(-\frac{\hbar^2}{2m} \nabla^2 + v_{eff}(\mathbf{r}) \right) \varphi_i(\mathbf{r}) = \varepsilon_i \varphi_i(\mathbf{r}), \tag{4.25}$$

and summing

$$n(\mathbf{r}) = \sum_i |\varphi_i(\mathbf{r})|^2. \tag{4.26}$$

The trick applied by Kohn and Sham was to compare the Euler-Lagrange equation for this non-interacting system with the one in an interacting system.

Using the index s on the kinetic energy functional $T_s[n]$ to remind us that it refers to the non-interacting (**s**ingle-electron) system, the energy functional $E[n]$ equals

$$E[n] = T_s[n] + V_{eff}[n] = T_s[n] + \int n(\mathbf{r}) v_{eff}(\mathbf{r}) d\mathbf{r}, \tag{4.27}$$

which, with the constraint from eq. (4.14) included by a Lagrange multiplier ε, yields the Euler-Lagrange equation

$$\begin{aligned} \frac{\delta E[n]}{\delta n} =& \frac{\delta T_s[n]}{\delta n} + \frac{\delta V_{eff}[n]}{\delta n} - \varepsilon \\ =& \frac{\delta T_s[n]}{\delta n} + v_{eff}(\mathbf{r}) - \varepsilon = 0. \end{aligned} \tag{4.28}$$

Meanwhile, the energy functional for the interacting system can, with some deliberate rearrangements, be written as

$$E[n] = T_s[n] + U_H[n] + E_{xc}[n] + E_{ext}[n], \tag{4.29}$$

where $U_H[n]$ is defined in eq. (4.12) and $E_{xc}[n]$ are the corrections needed to make $E[n]$ exact,

$$E_{xc}[n] = T[n] - T_s[n] + U_{int}[n] - U_H[n]. \tag{4.30}$$

Once again applying the variational principle with the constraint (4.14), gives

$$\begin{aligned} \frac{\delta E[n]}{\delta n} &= \frac{\delta T_s[n]}{\delta n} + \frac{\delta U_H[n]}{\delta n} + \frac{\delta E_{xc}}{\delta n} + \frac{\delta V_{ext[n]}}{\delta n} - \varepsilon \\ &= \frac{\delta T_s[n]}{\delta n} + e^2 \int \frac{n(\mathbf{r_1})}{|\mathbf{r} - \mathbf{r_1}|} d\mathbf{r_1} + v_{xc}(\mathbf{r}) + v_{ext}(\mathbf{r}) - \varepsilon = 0. \end{aligned} \tag{4.31}$$

Comparing eq. (4.28) and eq. (4.31), we realise they are identical if we choose

$$v_{eff}(\mathbf{r}) = \int \frac{n(\mathbf{r_1})}{|\mathbf{r} - \mathbf{r_1}|} d\mathbf{r_1} + v_{xc}(\mathbf{r}) + v_{ext}(\mathbf{r}), \tag{4.32}$$

which also was the purpose with the reshuffling made in eq. (4.29). The Kohn-Sham procedure can now be summarised in four steps,

I) initially guess a density $n_0(\mathbf{r})$

II) compute $v_{eff}(\mathbf{r})$ through eq. (4.32)

III) solve eq. (4.25) and compute a new density $n_0(\mathbf{r})$ through (4.26)

IV) repeat from step II until $n_0(\mathbf{r})$ is converged

However, the problem to find an explicit expression for the term $E_{xc}[n]$ in eq. (4.30) remains. This term should include all the corrections needed to make the energy functional $E[n]$ exact. Part of this correction is due to the Pauli principle[2] – the classical e-e energy $U_H[n]$ obviously do not take this into account. Part of the correction stems from the fact that the actual wave function can not, in general, be written as some combination of the functions ϕ_i in equation (4.25). These two contributions are often written separate, namely as an *exchange* (Pauli principle) and *correlation* (exact wave function) contribution,

$$E_{xc}[n] = E_x[n] + E_c[n]. \tag{4.33}$$

One of the more successful ways to approximate them is through the *Local Density Approximation* (LDA).

4.5 Local Density Approximation

In the case of a uniform electron gas the exchange and correlation energy per particle, $\varepsilon_x(n)$ and $\varepsilon_c(n)$, can be determined. In LDA it is then assumed that the total exchange-correlation energy for *any* system is the sum of these energies weighted with the local density, i.e.,

$$E_x[n] = \int \varepsilon_x[n] n(\mathbf{r}) d\mathbf{r} \tag{4.34}$$

$$E_c[n] = \int \varepsilon_c[n] n(\mathbf{r}) d\mathbf{r}. \tag{4.35}$$

An expression for $\varepsilon_x[n]$ was first proposed by Dirac as an improvement to the Thomas-Fermi model[8]. For a 2DEG[23],

$$\varepsilon_x[n] = -\frac{\sqrt{2}e^2}{3\pi^{\frac{3}{2}}\varepsilon_0}\sqrt{n(\mathbf{r})}, \tag{4.36}$$

where e is the electron charge and ε_0 the permittivity. A closed expression for the correlation part is a little bit more troublesome. Using Monte Carlo methods it may be computed exactly for different densities whereupon these values are interpolated to fit some analytical expression[21, 23, 24]. E.g., with the density parameter r_s defined as

$$r_s = \frac{1}{a_0\sqrt{\pi n}} \tag{4.37}$$

and a_0 being the Bohr radius, Tanatar and Cerperly proposed[23]

$$\varepsilon_c[n] = -\frac{C_0 e^2}{2 * 4\pi\varepsilon_0 a_0}\left(\frac{1 + C_1\sqrt{r_s}}{1 + C_1\sqrt{r_s} + C_2 r_s + C_3 (r_s)^{3/2}}\right) \tag{4.38}$$

[2]No two electrons in a given system can be in states characterised by the same set of quantum numbers.

where the coefficients C_i were determined from least square fits with their Monte Carlo simulations.

4.6 Local Spin Density Approximation

Density functional theory within LDA can be extended to include electron-spin effects using the *local spin density approximation* (LSDA). Equation (4.25) is now written as two equations,

$$\left(-\frac{\hbar^2}{2m}\nabla^2 + v^\sigma_{eff}(\mathbf{r})\right)\varphi^\sigma_i(\mathbf{r}) = \varepsilon_i\varphi^\sigma_i(\mathbf{r}), \tag{4.39}$$

where we differentiate between the two spin species $\sigma = \uparrow, \downarrow$. The spin-up/down densities are given by

$$n^\uparrow(\mathbf{r}) = \sum_i |\varphi^\uparrow_i(\mathbf{r})|^2 \tag{4.40}$$

and

$$n^\downarrow(\mathbf{r}) = \sum_i |\varphi^\downarrow_i(\mathbf{r})|^2 \tag{4.41}$$

and the total density

$$n(\mathbf{r}) = n^\uparrow(\mathbf{r}) + n^\downarrow(\mathbf{r}). \tag{4.42}$$

The effective potential $v^\sigma_{eff}(\mathbf{r})$ is

$$v^\sigma_{eff}(\mathbf{r}) = e^2\int\frac{n(\mathbf{r_1})}{|\mathbf{r}-\mathbf{r_1}|}d\mathbf{r_1} + v^\sigma_x(\mathbf{r}) + v^\sigma_c(\mathbf{r}) + v^\sigma_{ext}(\mathbf{r}). \tag{4.43}$$

The exchange energy per particle now depends on both spin up and spin down, $\varepsilon_x[n^\uparrow, n^\downarrow]$. This is usually rewritten using the polarisation parameter

$$\zeta = \frac{n^\uparrow - n^\downarrow}{n^\uparrow + n^\downarrow} \tag{4.44}$$

as $\varepsilon_x[n, \zeta]$, which may be expressed in terms of the unpolarised $\varepsilon_x[n]$. For a 2DEG[23]

$$\varepsilon_x[n,\zeta] = \frac{1}{2}\varepsilon_x[n]\left((1+\zeta)^{3/2} + (1-\zeta)^{3/2}\right). \tag{4.45}$$

The exchange potential $v^\sigma_x(\mathbf{r})$ is then given by the functional derivative

$$v^\sigma_x(\mathbf{r}) = \frac{\delta E_x[n,\zeta]}{\delta n^\sigma}, \tag{4.46}$$

where

$$E_x[n,\zeta] = \int n(\mathbf{r})\varepsilon_x[n,\zeta]d\mathbf{r}. \tag{4.47}$$

$v^\sigma_c(\mathbf{r})$ is similarly obtained from

$$v^\sigma_c(\mathbf{r}) = \frac{\delta E_c[n,\zeta]}{\delta n^\sigma}, \tag{4.48}$$

where a parameterisation for $\varepsilon_c[n, \zeta]$ can be found in[1].

Chapter 5

Modelling

5.1 Tight-binding Hamiltonian

Let $|m,n\rangle$ be the direct product, $|m\rangle \otimes |n\rangle = |m\rangle|n\rangle = |mn\rangle$, representing a state centred at site m,n in the discretisation of the 2D semi-infinite waveguide shown in figure 5.1. The $|m,n\rangle$ fulfills the relationship for completeness and orthonormality

$$\sum_{m,n} |m,n\rangle\langle m,n| = 1 \quad \text{and} \quad \langle m,n|m',n'\rangle = \delta_{mn,m'n'}. \tag{5.1}$$

An arbitrary state $|\Psi\rangle$ can be expanded in this basis as

$$|\Psi\rangle = \sum_{m,n} c_{mn}|m,n\rangle, \tag{5.2}$$

where $|c_{mn}|^2$ is the probability to find the electron at site m,n. The *tight-binding Hamiltonian* for an electron moving in a perpendicular magnetic field may now be written as

$$\begin{aligned}\hat{H} = \sum_{m,n} \Big[& |m,n\rangle \left(\varepsilon_0 + V_{mn}\right) \langle m,n| \\ & + |m,n\rangle t \langle m,n+1| + |m,n\rangle t \langle m,n-1| \\ & + |m,n\rangle t e^{-iqn} \langle m+1,n| + |m,n\rangle t e^{iqn} \langle m-1,n| \Big].\end{aligned} \tag{5.3}$$

V_{mn} is the on-site potential, ε_0 the on-site energy, t the hopping integral between sites and the phase factor $e^{\pm iqn}$ comes from inclusion of a perpendicular magnetic field (Landau gauge) via Peierl's substitution[11, 12]. With the choice of

$$\varepsilon_0 = \frac{2\hbar^2}{m^* a^2}, \qquad t = -\frac{1}{4}\varepsilon_0, \qquad q = \frac{eBa^2}{\hbar}, \tag{5.4}$$

m^* being the effective electron mass, e the electron charge, B the magnetic field and a the lattice discretisation constant, eq. (5.3) converges to its continuous counterpart as $a \to 0$.

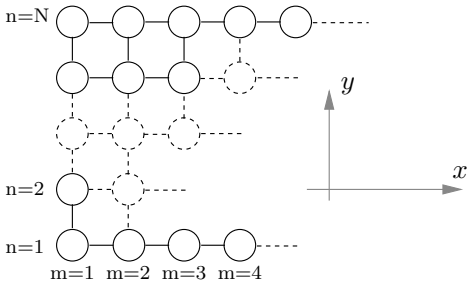

Figure 5.1: Discretisation of a two-dimensional semi-infinite quantum waveguide with transversal sites indexed from $n{=}1 \ldots N$ and longitudinal sites $m{=}1 \ldots \infty$.

5.1.1 Mixed representation

Working with quantum wires, it is sometimes convenient to pass from the real space representation with the states $|m, n\rangle$ to a mixed state representation using the transversal lead eigenfunctions (c.f. with the continuous case in eq. 2.23),

$$\varphi_n = \sqrt{\frac{2}{N+1}} \sin\left(\frac{\pi n \alpha}{N+1}\right) \qquad \alpha \in \mathbb{N}. \tag{5.5}$$

Denoting these states $|m, \alpha\rangle$, where m signifies the longitudinal position and α the transverse mode we can write the transformation between $|m, n\rangle$ and $|m, \alpha\rangle$ as

$$\begin{aligned} |m,\alpha\rangle &= \sum_{m',n'} \Big(|m',n'\rangle\langle m',n'|\Big)|m,\alpha\rangle \\ &= \sum_{m',n'} |m',n'\rangle\Big(\langle m',n'|m,\alpha\rangle\Big) = \sum_{n'}\langle n'|\alpha\rangle|m,n'\rangle \\ &= \sum_{n'} \sqrt{\frac{2}{N+1}} \sin\left(\frac{\pi n' \alpha}{N+1}\right)|m,n'\rangle. \end{aligned} \tag{5.6}$$

5.1.2 Energy dispersion relation

We will now consider the energy dispersion relation for the tight-binding Hamiltonian in zero magnetic field. Expanding the solution $|\Psi\rangle$ to eq. (5.3) as

$$|\Psi\rangle = \sum_{m,\alpha} \psi_{mn}|m,n\rangle \tag{5.7}$$

and substituting this back into eq. (5.3) yields

$$\varepsilon_0\psi_{mn} + t\psi_{m+1,n} + t\psi_{m-1,n} + t\psi_{m,n+1} + t\psi_{m,n-1} = E. \tag{5.8}$$

With the discussion of the quantum wire in section 2.3.2 in mind we assume a separable solution on the form

$$\psi_{mn} = \phi_m \varphi_n, \tag{5.9}$$

with corresponding longitudinal and transverse energy components,

$$E = E_\parallel + E_\perp = E_{k_\parallel} + E_\alpha. \tag{5.10}$$

After some rearrangements and writing out ε_0 and t from eq. (5.4) we get

$$-\frac{\hbar^2}{2m^*}\left(\frac{\phi_{m+1} - 2\phi_m + \phi_{m-1}}{a^2}\right) = E_{k_\parallel}\phi_m, \tag{5.11}$$

$$-\frac{\hbar^2}{2m^*}\left(\frac{\varphi_{n+1} - 2\varphi_n + \varphi_{n-1}}{a^2}\right) = E_\alpha \varphi_n. \tag{5.12}$$

These are discrete derivatives, and we will get travelling wave solutions in the parallel direction and quantised solutions in the transverse direction,

$$\phi_m = e^{ik_\parallel ma} \qquad k_\parallel \in \mathbb{R} \tag{5.13}$$

$$\varphi_n = \sqrt{\frac{2}{N+1}}\sin\left(\frac{\pi n \alpha}{N+1}\right) \qquad \alpha \in \mathbb{N}. \tag{5.14}$$

Substituting ϕ_m back into eq. (5.11) we get the dispersion relation in the longitudinal direction as

$$E_{k_\parallel} = \frac{\hbar^2}{2m^*a^2}\left(2 - 2\cos(k_\parallel a)\right). \tag{5.15}$$

If $k_\parallel a \ll 1$ this approximates to the continuous dispersion relation (see figure 5.2),

$$E_{k_\parallel} \approx \frac{\hbar^2}{2m^*a^2}\left(2 - 2\left(1 - \frac{(k_\parallel a)^2}{2}\right)\right) = \frac{\hbar^2(k_\parallel a)^2}{2m^*a^2} = \frac{\hbar^2 k_\parallel^2}{2m^*}. \tag{5.16}$$

Repeating the procedure for (5.14) in (5.12) yields an E_α,

$$E_\alpha = \frac{\hbar^2}{2m^*a^2}\left(2 - 2\cos\left(\frac{\pi\alpha}{N+1}\right)\right) \approx \frac{\hbar^2}{2m^*a^2}\left(\frac{\pi\alpha}{N+1}\right)^2 = \frac{\hbar^2\pi^2\alpha^2}{2m^*w^2}, \tag{5.17}$$

where $w = a(N+1)$ is the width of the channel. A comparison with eq. (2.24) identifies $\alpha\pi/w$ as $k_\perp$.

5.1.3 Group velocity

Knowing the energy dispersion relation allows us to compute the group velocity, v_g, as

$$v_g = \frac{d\omega}{dk_\parallel} = \frac{1}{\hbar}\frac{dE}{dk_\parallel} = \frac{1}{\hbar}\frac{d}{dk_\parallel}\left(\frac{\hbar^2}{2m^*a^2}\left(2 - 2\cos(k_\parallel a)\right)\right) = \frac{\hbar}{m^*a}\sin(k_\parallel a). \tag{5.18}$$

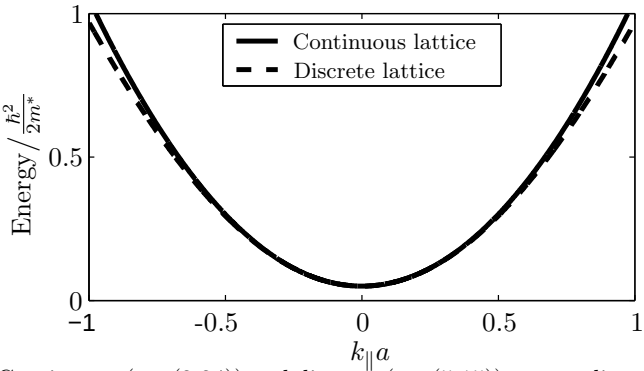

Figure 5.2: Continuous (eq. (2.24)) and discrete (eq. (5.15)) energy dispersion relation for the lowest subband.

5.2 Green's function

The S-matrix technique briefly mentioned in section 3.3.1 gives the response of a system at the boundary due to some excitation at the boundary. This section introduces the more powerful Green's function technique which gives the response of the system at *any* point due to an excitation at any point. This will allow us not only to compute the transmission coefficients through the dot but also the electron density inside the system.

5.2.1 Definition of Green's function

Given a differential operator $\mathcal{D}_{op}$ which relates an excitation $\mathcal{S}$ in some system to the system response $\mathcal{R}$ by

$$\mathcal{D}_{op}\mathcal{R} = \mathcal{S}, \tag{5.19}$$

the Green's function is defined as

$$\mathcal{G} = \mathcal{D}_{op}^{-1}. \tag{5.20}$$

Describing an electron travelling in a lead towards a quantum system as a unit excitation I at the system boundary, the Green's function is defined by

$$\mathsf{H}\Psi + I = \mathsf{E}\Psi \tag{5.21}$$

$$(\mathsf{E} - \mathsf{H})\Psi = I \tag{5.22}$$

$$\Psi = (\mathsf{E} - \mathsf{H})^{-1} I \tag{5.23}$$

$$\Rightarrow \quad \mathcal{G} = \Psi = (\mathsf{E} - \mathsf{H})^{-1}. \tag{5.24}$$

This definition actually allows two possible Green's functions, the *retarded* and the *advanced* Green's function. The former describes the wave function caused

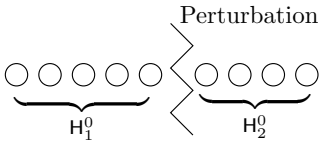

Figure 5.3: Two systems with respective Hamiltonian H_1^0 and H_2^0 separated by a perturbation.

by the excitation while the latter describes the wave function that generates the excitation. Evidently our interest lies in the retarded Green's functions and this may technically be specified by adding a small imaginary part to the energy[4],

$$\mathcal{G} = (\mathsf{E} - \mathsf{H} + i\delta)^{-1}. \tag{5.25}$$

5.2.2 Dyson equation

The most straightforward way to numerically calculate the Green's function is to perform the inverse in equation (5.24). However, matrix inversion is computationally a very expensive operation and a more manageable approach is to compute the Green's function recursively through the *Dyson equations*. Considering two adjacent systems H_1^0 and H_2^0, figure 5.3, and treating hopping between them as a small perturbation V, we can write the Hamiltonian for the combined system as

$$\mathsf{H} = \underbrace{\mathsf{H}_1^0 + \mathsf{H}_2^0}_{=\mathsf{H}^0} + V = \mathsf{H}^0 + V. \tag{5.26}$$

From equation (5.24) we have

$$\mathcal{G}^{-1} = \mathsf{E} - \mathsf{H} = \mathsf{E} - \mathsf{H}^0 - V = \left(\mathcal{G}^0\right)^{-1} - V, \tag{5.27}$$

where $\mathcal{G}^0$ is the Green's function of H^0. Multiplying equation (5.27) with $\mathcal{G}^0$ from the right and $\mathcal{G}$ from the left (or vice versa) yields the Dyson equation(s)

$$\mathcal{G} = \mathcal{G}^0 + \mathcal{G}^0 V \mathcal{G} \tag{5.28}$$

$$(\mathcal{G} = \mathcal{G}^0 + \mathcal{G} V \mathcal{G}^0). \tag{5.29}$$

These equations implicitly define $\mathcal{G}$ in terms of the known, unperturbed, $\mathcal{G}^0$. For explicit expressions for the Green's function between two specific points $\mathbf{r}$,$\mathbf{r}'$, we introduce the notation

$$\mathcal{G}(\mathbf{r}, \mathbf{r}') = \langle \mathbf{r}|\mathcal{G}|\mathbf{r}'\rangle = \langle m, n|\mathcal{G}|m', n'\rangle = \mathcal{G}_{mn,m'n'}. \tag{5.30}$$

Similarly $\mathcal{G}_{mm'}$ is interpreted as $\langle m|\mathcal{G}|m'\rangle$. The matrix $\mathcal{G}_{mm'}$ can then be written as

$$\mathcal{G}_{mm'} = \mathcal{G}^0_{mm'} + \sum_{i,j} \mathcal{G}^0_{mi} V_{ij} \mathcal{G}_{jm'}. \tag{5.31}$$

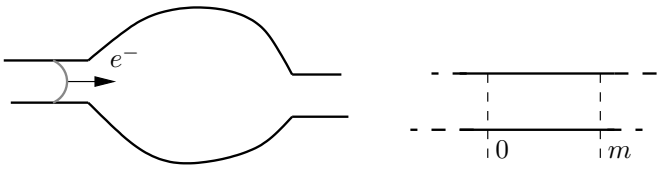

(a) (b)

Figure 5.4: **(a):** Typical system under consideration, two leads are connecting the quantum dot to an electron reservoirs at infinity. An incoming electron e^- from the right may either be reflected back to the left lead or transmitted to the right. **(b):** A straight, homogenous channel with zero magnetic field.

For two systems labelled 1 and 2 we have

$$\mathsf{H} = \mathsf{H}_{01} + \mathsf{H}_{02} + V = \mathsf{H}_0 + V_{12} + V_{21} \tag{5.32}$$

where

$$V_{12} = |1\rangle t_{12} \langle 2| = |1\rangle t e^{iqn} \langle 2| \tag{5.33}$$

$$V_{21} = |2\rangle t_{21} \langle 1| = |2\rangle t e^{-iqn} \langle 1|. \tag{5.34}$$

The Green's functions for the combined function may now be found through eq. (5.31). For example,

$$\mathcal{G}_{11} = \mathcal{G}^0_{11} + \mathcal{G}^0_{11} V_{12} \mathcal{G}_{21} \tag{5.35}$$

$$\mathcal{G}_{21} = \underbrace{\mathcal{G}^0_{21}}_{=0} + \mathcal{G}^0_{22} V_{21} \mathcal{G}_{11}, \tag{5.36}$$

substituting back and forth yields, after some rearrangements

$$\mathcal{G}_{11} = (I - \mathcal{G}^0_{11} V_{12} \mathcal{G}^0_{22} V_{21})^{-1} \mathcal{G}^0_{11} \tag{5.37}$$

$$\mathcal{G}_{21} = \mathcal{G}^0_{22} V_{21} (I - \mathcal{G}^0_{11} V_{12} \mathcal{G}^0_{22} V_{21})^{-1} \mathcal{G}^0_{11}. \tag{5.38}$$

In a similar way expressions to add entire sections of recursively computed Green's functions, such as in figure 5.5 and 5.8, can be derived.

5.2.3 Surface Green's function

Using eq. (5.31) above, we can find the full Green's function for a finite system by recursively adding parts of the system together. However, usually the system we will consider is infinite, as in figure 5.4**a**, and the Green's function in the leads has to be computed in some other way. For a straight, hard wall potential channel with zero magnetic field the solutions to the Shrödinger

equation is given by eq. (5.13) and (5.14). An excitation $\psi_{0\alpha}|m,\alpha\rangle$ at slice 0 in figure 5.4**b** gives the response

$$|\Psi\rangle = \mathcal{G}\psi_{0\alpha}|0,\alpha\rangle. \tag{5.39}$$

Because there can be no mixing between different modes α in a homogenous wire we temporarily suppress index α and write $|m,\alpha\rangle \to |m\rangle$. $|\Psi\rangle$ is now expanded as

$$|\Psi\rangle = \sum_m \psi_m|m\rangle = \mathcal{G}\psi_0|0\rangle. \tag{5.40}$$

Multiplying from the right with $\langle m|$ gives the response at site m

$$\psi_m = \langle m|\mathcal{G}\psi_0|0\rangle = \mathcal{G}_{m0}\psi_0. \tag{5.41}$$

From the Dyson equation (5.29) we find $\mathcal{G}_{m+1,0}$ as

$$\mathcal{G}_{m+1,0} = \underbrace{\mathcal{G}^0_{m+1,0}}_{=0} + \mathcal{G}^0_{m+1,m+1}V_{m+1,m}\mathcal{G}_{m0} \tag{5.42}$$

and thereby

$$\psi_{m+1} = \mathcal{G}_{m+1,0}\psi_0 = \mathcal{G}^0_{m+1,m+1}V_{m+1,m}\mathcal{G}_{m0}\psi_0 \underset{\textbf{eq. (5.41)}}{=} \mathcal{G}^0_{m+1,m+1}V_{m+1,m}\psi_m. \tag{5.43}$$

The potential in the wire is periodic and we apply the Bloch theorem,

$$\psi_m = e^{ik_\parallel^\alpha ma}u_m, \tag{5.44}$$

where u_m is periodic, $u_m = u_{m+1}$, and $k_\parallel^\alpha$ is the wave vector from eq. (2.24) associated with the transverse mode α. From eq. (5.43) we get

$$e^{ik_\parallel^\alpha(m+1)a} = \mathcal{G}^0_{m+1,m+1}V_{m+1,m}e^{ik_\parallel^\alpha ma} \tag{5.45}$$

$$e^{ik_\parallel^\alpha a} = \mathcal{G}^0_{m+1,m+1}V_{m+1,m}. \tag{5.46}$$

Defining the surface Green's function as $\tilde{\Gamma} = G^0_{m+1,m+1}$, where tilde reminds us that this is in mixed representation and noting that for zero magnetic field $V_{m+1,m} = t$, we obtain,

$$e^{ik_\parallel^\alpha a} = t\tilde{\Gamma}. \tag{5.47}$$

With all N modes $\alpha_1, \alpha_2, \ldots, \alpha_N$, the surface Green's function is a diagonal matrix

$$\tilde{\mathbf{\Gamma}} = \frac{1}{t}\begin{pmatrix} e^{ik_\parallel^{\alpha_1}a} & 0 & \cdots & \\ 0 & e^{ik_\parallel^{\alpha_2}a} & 0 & \\ \vdots & 0 & \ddots & \\ & & & e^{ik_\parallel^{\alpha_N}a} \end{pmatrix} \tag{5.48}$$

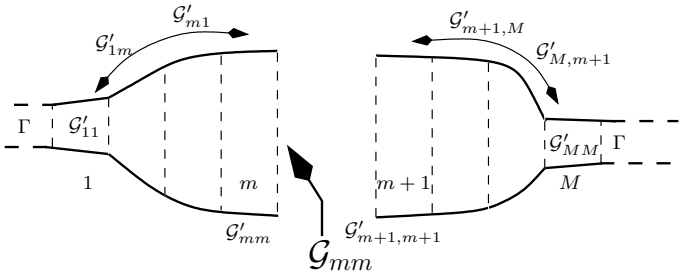

Figure 5.5: Recursively adding slices by eq. (5.31) from right and left lead we may compute the Green's function at slice m, $\mathcal{G}_{mm}$, for the full system. The diagonal elements of $\Im\big[\mathcal{G}_{mm}\big]$ is proportional to the density of states (eq. (5.50)).

which may be transformed to real space representation by

$$\begin{aligned}\Gamma(mn, m'n') = \langle mn|\Gamma|m'n'\rangle &= \langle n|\Gamma_{mm'}|n'\rangle \\ &= \sum_{\alpha,\alpha'}\langle n||\alpha\rangle\langle\alpha|\Gamma_{mm'}|\alpha'\rangle\langle\alpha'||n'\rangle \\ &= \sum_{\alpha,\alpha'}\langle\alpha|n\rangle^*\tilde{\Gamma}(m\alpha, m'\alpha')\langle\alpha'|n'\rangle, \quad (5.49)\end{aligned}$$

where '$*$' denotes the complex conjugate.

5.2.4 Computational procedure

Figure 5.5 schematically shows the recursive Green's function technique applied to a two-lead quantum dot. The dot is divided into M slices; the Green's function for each slice is described by the matrix $\mathcal{G}_{kk}$ while the Green's function between slice k and l by the matrices $\mathcal{G}_{kl}$ and $\mathcal{G}_{lk}$. Starting from the surface Green's function Γ, we recursively add slice by slice until we have computed the Green's functions $\mathcal{G}'_{mm}$ and $\mathcal{G}'_{m+1,m+1}$ indicated in figure 5.5. Using the Dyson equation we may now compute the total Green's function $\mathcal{G}_{mm}$ for slice m. The imaginary part of the diagonal elements in this matrix ($\Im[\mathcal{G}(\mathbf{r},\mathbf{r})]$) are proportional to the density of states[11],

$$n(E,\mathbf{r}) = -\frac{1}{\pi}\Im\Big[\mathcal{G}(\mathbf{r},\mathbf{r},E)\Big]. \quad (5.50)$$

Integrating the density of states up to the Fermi-energy we find the electron density inside the dot,

$$n(\mathbf{r}) = -\frac{1}{\pi}\Im\left[\int_{-\infty}^{E_f}\mathcal{G}(\mathbf{r},\mathbf{r},E)dE\right]. \quad (5.51)$$

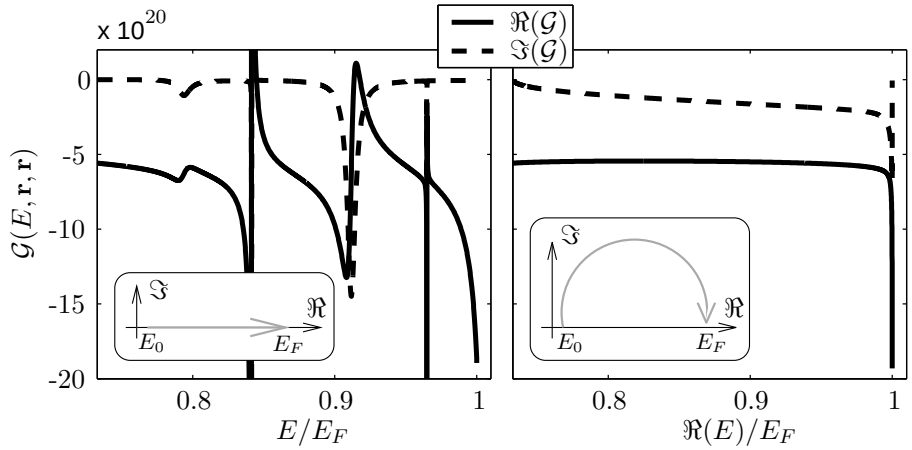

Figure 5.6: Real (solid line) and imaginary (dashed line) part of the Green's function at a single point m, n for a typical system. Left panel shows the Green's function along the real axis (gray arrow in inset, E_0 is the lowest potential in the dot, E_F the Fermi level). Because of the very sharp peaks numerical integration is difficult along this path. Right panel shows the Green's function along the path indicated by the gray arrow in the right inset. The Green's function is analytical in the upper half of the complex plane, hence integration along this path yields the same result as along the real axis but is numerically easier.

Using DFT in conjunction with the recursive Green's function technique we can now write down a procedure to find a self-consistent density to an arbitrary two-lead quantum dot.

I) guess an an initial density $n(\mathbf{r})$ (e.g., by Thomas-Fermi)

II) compute an effective potential $v_{eff}(\mathbf{r})$ by equation (4.32)

III) update the Hamiltonian (eq. (5.3)) with the new $v_{eff}(\mathbf{r})$

IV) update the Green's function with the new Hamiltonian (eq. (5.24))

V) update the density $n(\mathbf{r})$ through eq. (5.51)

VI) repeat from step II until $n(\mathbf{r})$ converges

There are some problems with convergence in this procedure. If the density between subsequent iterations varies too much, this may cause the solution to oscillate – this problem is typically addressed by mixing the new density with the old density by some parameter ϵ,

$$n_{new}(\mathbf{r}) = \epsilon n_{new}(\mathbf{r}) + (1-\epsilon) n_{old}(\mathbf{r}) \qquad 0 < \epsilon \leq 1, \tag{5.52}$$

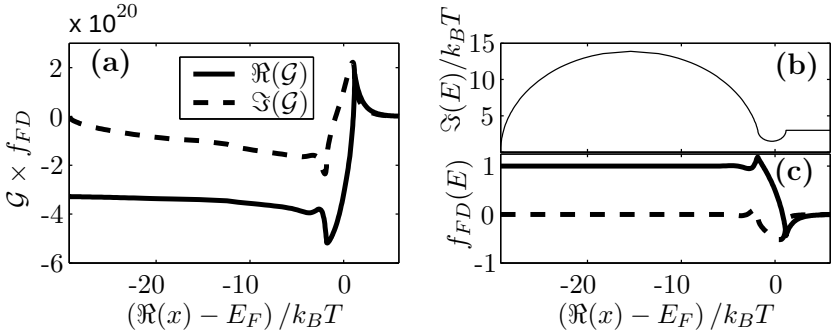

Figure 5.7: **(a)** Real and imaginary parts of Green's function at point m, n multiplied with the Fermi-Dirac distribution. **(b)** Integration path in complex plane. **(c)** Real and imaginary part of Fermi-Dirac distribution (f_{FD}) along the path in (b).

thereby dampening any sudden change in the density. Furthermore, the Green's function has some very sharp features along the real axis (see the left panel of figure 5.6), making numerical integration very difficult. Since all poles to the Green's function are below the real axis this may be remedied by carrying out the integration in the complex plane (see the right panel of figure 5.6), where the Green's function is far smoother.

This may however still not be enough for convergence. With a high density of states close to the Fermi level the Green's function may change steeply as we return towards the real axis, and the last part of the integration will require a very fine stepsize ΔE to capture the integral accurately. A simpler approach is to slightly increase the temperature in the system. With $T > 0K$ some states above the Fermi level E_F will be occupied and the density is given by

$$n_e(\mathbf{r}, E_F, T) = \int_{-\infty}^{\infty} \underbrace{n(E, \mathbf{r})}_{\text{DOS}} \underbrace{f_{FD}(E, E_F, T)}_{\text{F-Ddist.}} dE, \tag{2.27}$$

where f_{FD} is the Fermi-Dirac distribution. We may now continue the integration in the complex plane until the Green's function is suppressed by the exponentially decaying Fermi-Dirac distribution, see figure 5.7.

With the self-consistent density $n_{eff}(\mathbf{r})$ we compute the Green's function relating the first and last slice as shown in figure 5.8, $\mathcal{G}_{M1}$. In mixed representation this matrix gives the transmission amplitudes between mode α in the left lead to mode β in the opposite lead[11]

$$t_{\beta \leftarrow \alpha} = i2|t| \sqrt{\sin\left(k_\parallel^\alpha a\right) \sin\left(k_\parallel^\beta a\right)} e^{i(k_\parallel^\alpha m - k_\parallel^\beta n)} \tilde{\mathcal{G}}_{M\beta,1\alpha}(E), \tag{5.53}$$

where $\tilde{\mathcal{G}}_{M\beta,1\alpha}(E) = \langle M\beta|\tilde{\mathcal{G}}(E)|1\alpha\rangle$, and tilde indicates that it is the Green's function in mixed representation. The amplitude for the reflected electron is

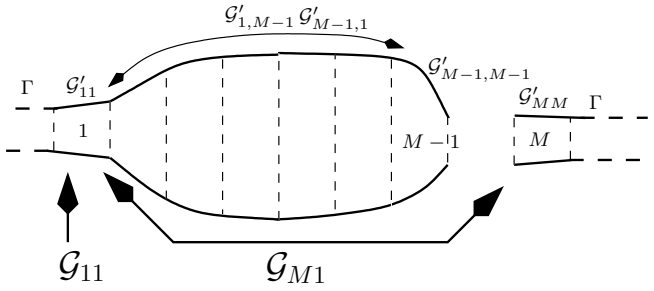

Figure 5.8: With the self-consistent density $n(\mathbf{r})$, we compute the Green's functions $\mathcal{G}_{M1}$ ($\mathcal{G}_{11}$) for the full system, which in mixed representation gives the transmission amplitudes by eq. (5.53) (reflection amplitudes by eq. (5.54)).

similarly[11]

$$r_{\beta\leftarrow\alpha} = i\sqrt{\sin\left(k_\parallel^\beta a\right) \Big/ \sin\left(k_\parallel^\alpha a\right)}\, e^{ia(k_\parallel^\beta + k_\parallel^\alpha)} \times \left[2|t| \sin\left(k_\parallel^\beta a\right) \tilde{\mathcal{G}}_{1\beta,1\alpha}(E) + i\delta_{\beta\alpha}\right], \quad (5.54)$$

where $\delta_{\alpha\beta}$ is the Dirac delta function.

Bibliography

[1] Claudio Attaccalite, Saverio Moroni, Paola Gori-Giorgi, and Giovanni B. Bachelet. Correlation energy and spin polarization in the 2d electron gas. *Phys. Rev. Lett.*, 88(25):256601, 2002.

[2] G. Binasch, P. Grünberg, F. Saurenbach, and W. Zinn. Enhanced magnetoresistance in layered magnetic structures with antiferromagnetic interlayer exchange. *Phys. Rev. B*, 39:4828, 1989.

[3] B.H. Bransden and C.J. Joachain. *Quantum Mechanics*. Prentice Hall, second edition, 2000.

[4] Supriyo Datta. *Electronic Transport in Mesoscopic Systems*. The press syndicate of the university of Cambridge, 1997.

[5] Supriyo Datta and Biswajit A. Das. Electronic analog of the electro-optic modulator. *Appl. Phys. Lett.*, 56:665, 1990.

[6] John H. Davies. *The physics of low-dimensional semiconductors*. The press syndicate of the university of Cambridge, 1998.

[7] P.A.M. Dirac. Quantum mechanics of many-electron systems. *Proc. Royal Soc. (**A**)*, 123(792):714, apr 1929.

[8] P.A.M. Dirac. Note on exchange phenomena in the thomas atom. *Proc. Cambridge Phil. Soc.*, 26:376, 1930.

[9] K.J. Thomas *et. al.* Transmission of interacting electrons throuh a one-dimensional periodic potential. *Phys. Rev. Lett.*, 77(1):135, 1996.

[10] M. N. Baibich *et al.* Giant magnetoresistance of (001)fe/(001)cr magnetic superlattices. *Phys. Rev. Lett.*, 61:2472, 1988.

[11] David K. Ferry and Stephen M. Goodnick. *Transport in nanostructures*. The press syndicate of the university of Cambridge, 1997.

[12] Richard P. Feynman, Robert B. Leighton, and Matthew Sands. *The Feynman lectures on physics*. Addison-Wesly Publishing Company, third edition, 1965.

[13] A. Ghosh, C. J. B. Ford, M. Pepper, H. E. Beere, and D. A. Ritchie. Possible evidence of a spontaneous spin polarization in mesoscopic two-dimensional electron systems. *Phys. Rev. Lett.*, 92(11):116601, mar 2004.

[14] P. Hohenberg and W. Kohn. Inhomogeneous electron gas. *Physical Review*, 136:B864, 1964.

[15] W. Kohn and L.J. Sham. Self-consistent equations including exchange and correlation effects. *Physical Review*, 140:A1133, 1965.

[16] Walter Kohn. Electronic structure of matter – wave functions and density functionals. *Nobel Lectures*, 1999.

[17] Leo Kouwenhoven and Leonid Glazman. Revival of the kondo effect. *Physics World*, page 33, 2001.

[18] G.E. Moore. Cramming more components onto integrated circuits. *Electronics*, 38(8), apr 1965. Also available at <http://www.intel.com/-research/silicon/moorespaper.pdf>.

[19] D.W. Palmer. The semiconductors-information web-site. www.semiconductors.co.uk, apr 2003.

[20] Robert G. Parr and Weitao Yang. *Density-Functional Theory of Atoms and Molecules*. Oxford University Press, 1989.

[21] John P. Perdew and Yue Wang. Accurate and simple analytic representation of the electron-gas correlation energy. *Phys. Rev. B*, 45(23):13244, 1992.

[22] Gary A. Prinz. Magetoelectrnoics. *Science*, 282(5394):1660, nov 1998.

[23] B. Tanatar and D.M. Ceperley. Ground state of the two-dimensional electron gas. *Phys. Rev. B*, 39(8):5005, 1989.

[24] U. von Barth and L.Hedin. A local exchange correlation potential for the spin poarized case:i. *J. Phys. C: Solid State Phys.*, 5:1629, 1972.